





Optofluidic chip with directly printed polymer optical waveguide Mach-Zehnder interferometer sensors for label-free biodetection

HAN WANG,¹ ZHITUO CHEN,^{1,2} TAIGE LI,¹ HUIMIN XIE,¹ BOHAN YIN,³ SIU HONG DEXTER WONG,³ YAOCHENG SHI,² 
AND A. PING ZHANG^{1,*} 

¹Photonics Research Institute, Department of Electrical and Electronic Engineering, The Hong Kong Polytechnic University, Kowloon, Hong Kong SAR, China

²Center for Optical and Electromagnetic Research, College of Optical Science and Engineering, International Research Center for Advanced Photonics, Zhejiang University, Hangzhou 310058, China

³Department of Biomedical Engineering, The Hong Kong Polytechnic University, Kowloon, Hong Kong SAR, China

*azhang@polyu.edu.hk

Abstract: Optofluidic devices hold great promise in biomedical diagnostics and testing because of their advantages of miniaturization, high sensitivity, high throughput, and high scalability. However, conventional silicon-based photonic chips suffer from complicated fabrication processes and less flexibility in functionalization, thus hindering their development of cost-effective biomedical diagnostic devices for daily tests and massive applications in responding to public health crises. In this paper, we present an optofluidic chip based on directly printed polymer optical waveguide Mach-Zehnder interferometer (MZI) sensors for label-free biomarker detection. With digital ultraviolet lithography technology, high-sensitivity asymmetric MZI microsensors based on a width-tailored optical waveguide are directly printed and vertically integrated with a microfluidic layer to make an optofluidic chip. Experimental results show that the sensitivity of the directly printed polymer optical waveguide MZI sensor is about 1695.95 nm/RIU. After being modified with capture molecules, i.e., goat anti-human immunoglobulin G (IgG), the polymer optical waveguide MZI sensors can on-chip detect human IgG at the concentration level of 1.78 pM. Such a polymer optical waveguide-based optofluidic chip has the advantages of miniaturization, cost-effectiveness, high sensitivity, and ease in functionalization and thus has great potential in the development of daily available point-of-care diagnostic and testing devices.

© 2024 Optica Publishing Group under the terms of the [Optica Open Access Publishing Agreement](#)

1. Introduction

Rapid and accurate detection of disease biomarkers at the point of care (POC) has become increasingly important for enhancing health care services and improving patient-centered outcomes [1–4]. It is particularly demanded to develop cost-effective biomedical diagnostic devices for daily testing and widespread applications in responding to public health crises. Currently the most common POC method is lateral flow immunoassay (LFIA) techniques because of their ease of use and short analysis time [5–8]. However, they can provide a qualitative result with limited sensitivity and specificity, compared to laboratory-based immunochemical methods. One of promising solutions to overcome these limitations is lab-on-a-chip (LoC) devices that integrate many kinds of microscale components to complete various processes on a chip scale. Particularly, integrated optofluidic chips that combines photonic microsensors with microfluidic components have been widely considered as the most promising solution for high-sensitivity biodetection because of the abundance of light-matter interactions as well as the high sensitivity and high signal-to-noise ratio of lightwave technology [9–12]. For instance,

Q. Liu *et al.* demonstrated a two-step sample-to-answer device with silicon Mach-Zehnder interferometer (MZI) sensors and a sample pretreatment module to detect malaria parasites [13]. X. Ouyang *et al.* developed an optofluidic chip with polymer whispering gallery mode (WGM) microlaser sensors for enzyme-linked immunosorbent assay (ELISA), which can detect vascular endothelial growth factor (VEGF) at the femtogram level [14].

Especially, optical waveguide-based photonic sensors hold great promises in the development of integrated optofluidic devices due to their well-known flexibility in on-chip integration [9,15]. They can guide light wave within a strip or rib with a very low propagation loss, and thus enable the creation of many kinds of micro-interferometers or micro-resonators to harness lightwave technology for high-sensitivity biosensing. Light wave is well confined within the guiding layer to make up interference or resonance with well-defined structures, meanwhile it may interact target molecules within surrounding medium via its evanescent field [16–18]. One of most widely used waveguide structures for bio-detection is MZI micro-sensors. Patricia. *et al.* proposed a MZI sensor based POC device for tuberculosis detection [19]. A photonic chip with six silicon nitride MZI sensors was fabricated and integrated with a disposable microfluidic cartridge for simultaneous detection of multiple disease biomarkers. It was demonstrated to detect tuberculosis in un-diluted urine at the concentration level of 475 pg/mL and its detection time is less than 15 mins. Densmore *et al.* demonstrated a silicon photonic MZI biosensor array for detection of two biomarkers at the same time [20]. Their results showed that the fabricated MZI sensor-based biochip could detect rabbit IgG and goat IgG simultaneously and the measured level of detection in terms of surface coverage is less than 0.3 pg/mm². Angelopoulou *et al.* developed an optofluidic chip combined with ten silicon MZI sensors and an advanced microfluidic module for simultaneous determination of four allergens, i.e., bovine milk protein, peanut protein, soy protein, and gliadin. It can complete analysis in 6.5 min, and its limits of detection for four allergens are 0.04 µg/mL, 1.0 µg/mL, 0.80 µg/mL and 0.10 µg/mL, respectively [21].

Polymer materials have advantages such as ease of manufacturing and modification as well as good biocompatibility, making them appealing for development of biomedical sensors and devices. For instance, Bruck *et al.* proposed a polymer MZI waveguide biochip, in which polyimide andOrmoclad were used to make core and cladding of polymer optical waveguide. Such a MZI waveguide sensor can measure streptavidin at the concentration of 0.1 µg/mL [22]. Paul *et al.* demonstrated a high-sensitivity SU-8 epoxy-based MZI biosensor, in which an extra ring resonator was introduced to enhance the sensitivity of the MZI optical biosensor via vernier effect. Such a sensor can achieve a sensitivity of above 17,000 nm/RIU in glucose solution measurement and its limit of detection is down to 1.1×10^{-6} RIU [23]. To fabricate high-quality optical waveguide sensors, one may use optical lithography [24], laser direct writing [25], or e-beam lithography technologies [26]. Although conventional optical lithography offers an efficient way to fabricate polymer optical waveguides, its process depends on a pre-prepared photomask and lacks grey-scale exposure ability. Laser direct writing and e-beam lithography technologies can overcome these technical bottlenecks to some extent but are commonly less efficient due to their inherent single-spot scanning nature.

In this paper, we present a polymer optical waveguide MZI sensor-integrated optofluidic biochip for label-free detection of disease biomarkers, which has become increasing important for the assessment of health, disease, or vaccination status in modern medical diagnostics, as shown in Fig. 1. With an own-developed digital ultraviolet lithography (DUL) technology [14, 27,28], an asymmetric MZI microsensor based on width-tailored optical waveguide is directly printed on a SiO₂/Si wafer for on-chip biosensing. A PDMS-based microfluidic layer is also fabricated by using DUL-based technology for packaging the optical waveguide chip to make an optofluidic chip. In the experiments, the fabricated optofluidic biochips showed a very high bulk sensitivity and can detect human immunoglobulin G (HIgG) at the concentration level of 1.78

pM. Moreover, it was demonstrated that the optofluidic chip can be repeatedly used multiple times and thus is promising to be developed towards reusable biodetection devices.

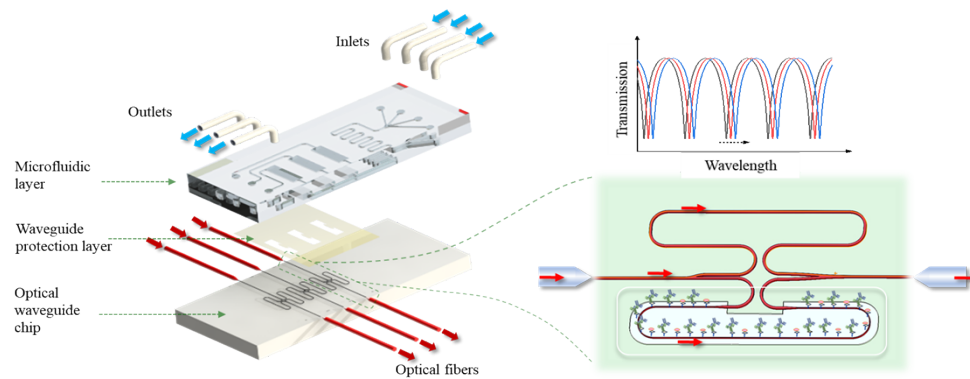


Fig. 1. Schematic of an optofluidic chip with multiple directly printed polymer optical waveguide MZ micro-interferometer sensors.

22. Methods and materials

2211 Materials

SS-LE2005 and 60 nm diameter were purchased from Kyokko Kakyokai, A Materials Materials, Inc. of USA. was ordered from Merck Reagents, Inc. Micro Grafting Technology and GmbH, Germany, provided, glycidyl methacrylate, propylene glycol dimethyl ether (PGME), (3-aminophenyl) acetate (APTES) and propyl triethoxysilane (BSPA) were purchased from Sigma-Aldrich (USA). Polydimethylsiloxane (PDMS) (Dow) and its curing agent were obtained from Dow Corning (USA) and HgCat, anti-human immunoglobulin G (IgG) and HlgG were purchased from Beijing Solarbio Science & Technology Co., Ltd., China.

2.2 Fabrication of SU-8 optical waveguide Mach-Zehnder interferometer sensors

2.2. Fabrication of SU-8 optical waveguide Mach-Zehnder interferometer sensors

The polymer optical waveguide sensors were fabricated by an own-developed DUL system, which was built with a high-power UV light-emitting diode (L10561-215; Hamamatsu Photonics, Japan), a high-speed digital micromirror device (DMD; DLP6500; Digital Light Processing Corp., USA), a microcomputer device (DMD; Dahe900; Digital Light Innovations, USA) and a high-speed digital micromirror device (DMD; Dahe900; Digital Light Innovations, USA) and a nanoprecision motorized stage (ANT130-XY; Aerotech Inc., USA) and a set of projection optics.

[illegible]

A cladding layer was fabricated by using another commercial power supply, Ormoclad Plasma cleaning was conducted using PUUTO Plasma Cleaner (PUUTOVA, Shanghai, China) with power of 200 W for 5 min. The air pressure was set at 200 Pa and 200 Pa and 100 Pa/min, respectively. Then, Ormoclad was grown on the top of the fabricated SU-8 waveguide chips. The overlay exposure function of the DUL system was used to precisely expose the Ormoclad over optical waveguide to form a cladding layer, while leaving a window upon sensing arm for optofluidic biosensing. A transition zone with the width of $\sim 90 \mu\text{m}$ were adopted during

function of the DUL system was used to precisely expose theOrmoclad over optical waveguide to form a cladding layer, while leaving a window upon sensing arm for optofluidic biosensing. A transition zone with the width of $\sim 90\text{ }\mu\text{m}$ were adopted during exposure of each sub-pattern to alleviate the shrinkage problem of Ormoclad during exposure. After a post-bake at $130\text{ }^{\circ}\text{C}$ for 15 min, the sample was developed by using methyl isobutyl ketone (MIBK). Finally, the optical waveguide chip was hard baked at $150\text{ }^{\circ}\text{C}$ for 3 h.

2.3. Fabrication of the optofluidic chip by packaging the waveguide chip with a microfluidic layer

The microfluidic layer was fabricated by using a casting method. The mold of microchannels was also prepared with SU-8. Poly(dimethylsiloxane) (PDMS) monomer was mixed with a cross-linking agent in 10:1 ratio and then degassed for 30 min. Then, PDMS was poured upon the SU-8 mold and baked at $70\text{ }^{\circ}\text{C}$ for 2 h to achieve completely cross-linking. Finally, the cured PDMS was peeled off from the SU-8 mould.

Both the PDMS layer and waveguide chip were first treated with plasma at the power of 200 W for 30 s. To prevent potential leakage between Ormoclad and substrate, some liquid PDMS was smeared around the edge of Ormoclad layer. The PDMS layer was then attached upon the waveguide chip with the help of a home-made alignment apparatus. Pressed with a clamp, the optofluidic chip was then baked in an oven at $70\text{ }^{\circ}\text{C}$ for 3 h to enhance the bonding between the waveguide chip and PDMS microfluidic channel layer.

2.4. Measurement of the transmission spectra of optical waveguide MZI sensors

The spectral responses of the fabricated polymer optical waveguide chip were measured by using an end-fire coupling setup. Light was launched from an ASE light source (at C band, i.e., $1530\sim 1560\text{ nm}$) into the optical waveguide chip by using a lensed single-mode optical fibre (SMF). The transmitted light was coupled into optical fibre by using another lensed SMF and its spectra was measured by using an optical spectrum analyzer (AQ6374, Yokogawa Company, Japan).

2.5. Functionalization of optical waveguide MZI sensors for label-free biodetection

The surface of the fabricated MZI sensors was activated to hydrophilic by using oxygen plasma [24], when it was packaged with microfluidic layer. To functionalize MZI sensors, 4% APTES aqueous solution was first injected into the microchannel of optofluidic chip to salinize the sensing arm for about 20 mins. Then, the sensing window was flushed with Phosphate-buffered saline (PBS) buffer solution. Subsequently, $100\text{ }\mu\text{g/mL}$ goat anti-human IgG was injected to incubate the sensing arm at room temperature for about 30 min. After washing out the unbound detection antibody, 1% BSA solution was injected to block the nonspecific site. Finally, PBS buffer solution was injected to wash out loosely bounded molecules, the MZI biosensor is ready for HIgG detection.

3. Results

3.1. Directly printed polymer asymmetric MZI microsensors with width-tailored optical waveguide

The fabricated SU-8 waveguide MZI sensors are shown in Fig. 2(a)-(d). SU-8 ($n = 1.573$) [29], Ormoclad ($n = 1.52$) [30], and SiO_2 ($n = 1.45$) were chosen to make the core, cladding, and substrate of the optical waveguide, respectively. The size of the SU-8 waveguide except sensing arm is chosen to $2\text{ }\mu\text{m}$ (height) $\times 2.7\text{ }\mu\text{m}$ (width), as shown in the inset of Fig. 2(a), which can make the waveguide not only work under single mode condition but also possess a relatively weak evanescent field for suppressing the optical loss caused by the Ormoclad cladding fabricated by direct printing processes. The width of the optical waveguide of sensing arm is narrowed to 2.1

μm , as shown in the inset of Fig. 2(b), to enhance its evanescent field for a better sensitivity. According to the numerical simulation given in Fig. S1, the evanescent field of the fundamental guided mode of the designed SU-8 waveguide can enter external water environment about 744 nm, which is sufficient to cover most of biomarkers in biological detection applications.

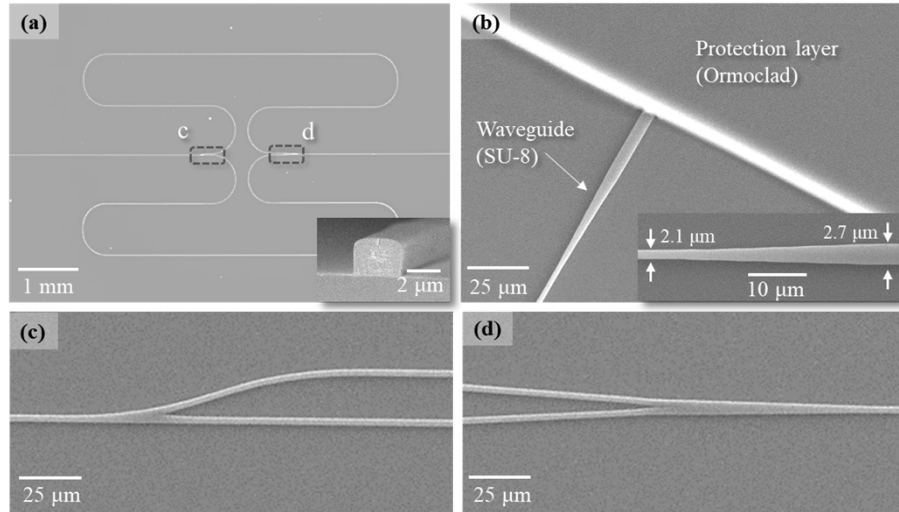


Fig. 2. (a) Optical micrograph image of the MZM mirror, inset is interference of waveguide, (b) SEM image of waveguide covered by Ormocoat, inset is enlarge of the tapered waveguide (c) a 1:2 splitter, and (d) a 1:1 splitter.

To minimize the mode mismatch induced optical propagation loss, an adiabatic taper with the length of 50 μm (Fig. 2(b)) is introduced between two different width waveguides. Since

the power of the light decreases after transmission through the reference and habiting tapes with the long difference of 50 μm (Fig. 12b) is optically added between the two different especially waveguides. Since the waveguide the signing is a fiber first. Its light of light is the waveguide. MZII has been specially designed with an different optical device to compensate the light power difference. The two light waveguides propagate through the fastings splitter of the optical respectively. MZII has been specially designed with a combiner structure to compensate the light power difference. The two light

waves propagating through the sensing and reference arms, respectively, the effective refractive indices of the output Y mode fiber. The sensing arm depends on the concentration of analyte. A change of

When the sensing arm is immersed in a solution of liquid with analyte, the effective refractive index of the optical modes of the sensing propagating through the sensing arm of analyte. A change of analyte concentration will cause a variation of the effective refractive index and lead to a change of optical phase of the light wave propagating through the sensing arm. If the wavelength of a spectral dip in transmission spectrum is employed as an output signal, the wavelength shift $\Delta\lambda$ given [31,32]:

caused by a change of the refractive index in the working section of sensing arm, which can be given [31,32]:

$$\Delta\lambda = \frac{\lambda L_1 \Delta n_{e1}}{\bar{r}} \quad (1)$$

$$\Delta\lambda = \frac{n_{g2}\bar{L}_{\lambda L_1\Delta n_{e1}} + n_{e1}\tilde{L}_1 - n_{g2}L_2}{\lambda L_1\Delta n_{e1}} \quad (1)$$

where \tilde{L}_1 , Δn_{e1} , and n_{g1} are the length, the induced change of effective refractive index, the group refractive index of the g_1 waveguide, and the group refractive index of the g_2 waveguide, respectively. \tilde{L}_2 and n_{g2} are the length and the group refractive index of the g_2 waveguide, respectively. \tilde{L}_1 and \tilde{L}_2 are the lengths of the embedded part of sensing arm and the reference arm, respectively. \tilde{L}_1 and \tilde{L}_2 are the lengths of the embedded part of sensing arm and the reference arm, respectively.

The measurement range of the waveguide MZI sensor depends on the free spectral range (FSR):

$$FSR = \frac{\lambda^2}{|n_{\sigma} \bar{L}_1 + n_{\sigma} \tilde{L}_1 - n_{\sigma} L_2|}. \quad (3)$$

The measurement range of the waveguide MZI sensor depends on the free spectral range (FSR):

$$FSR = \frac{\lambda^2}{|n_{g2}\tilde{L}_1 + n_{g1}\tilde{L}_1 - n_{g2}L_2|}. \quad (2)$$

If further consider the dependence of the effective refractive index of the working section of sensing arm on the refractive index of external medium, i.e., $\partial n_{e1}/\partial n_{ext}$, the bulk sensitivity S of the waveguide MZI sensor can be written as

$$S = \frac{FSR \cdot \tilde{L}_1}{\lambda} \cdot \frac{\partial n_{e1}}{\partial n_{ext}}, \quad (3)$$

where n_{ext} refers to the refractive index of external medium around the working section of sensing arm. In our design of MZI sensors, the length of the working section and embedded section of the sensing arm, i.e., \tilde{L}_1 and \tilde{L}_1 , and the length of reference arm L_2 are chosen to be 10.636 mm, 3.410 mm, and 13.918 mm, respectively. According to the numerical simulation, the group refractive indexes of the 2.1- μm wide sensing waveguide in water and the group refractive index of the 2.7- μm wide waveguide embedded in Ormoclade, i.e., n_{g1} and n_{g2} , are 1.6028 and 1.5805, respectively. Moreover, it was calculated that a change of 6×10^{-4} in external refractive index caused an increase of 2.5×10^{-5} in the effective refractive index of the 2.1- μm wide sensing waveguide. Correspondingly, the wavelength shift of the spectral dip can be calculated from Eqn. (1) to be 0.936 nm. The sensitivity of the MZI sensor can be estimated by Eqn. (3) to be 1560 nm/RIU at the wavelength of 1550 nm.

3.2. Microfluidic layer and optical waveguide chip vertically integrated optofluidic chip

The optical waveguide chip before and after vertical integration with a microfluidic layer is shown in Fig. 3. Figure 3(a) shows the photo of a fabricated SU-8 optical waveguide incident with red light. It can be seen that a cladding layer has been printed along with optical waveguide and a sensing window has been opened for vertical integration of microfluidic layer for detecting analytes in liquid sample. Figure 3(b) shows a fully packaged optofluidic chip. The optofluidic chip includes four inlets, one serpentine mixer and three outlets which are designed for injection, mixing and collection of waste liquids, respectively. Fig. S3 shows the fabricated SU-8 mold. In our experiments, these four inlets are used to inject functionalization solution, target molecule solution, washing buffer solution, and an antibody strip buffer respectively.

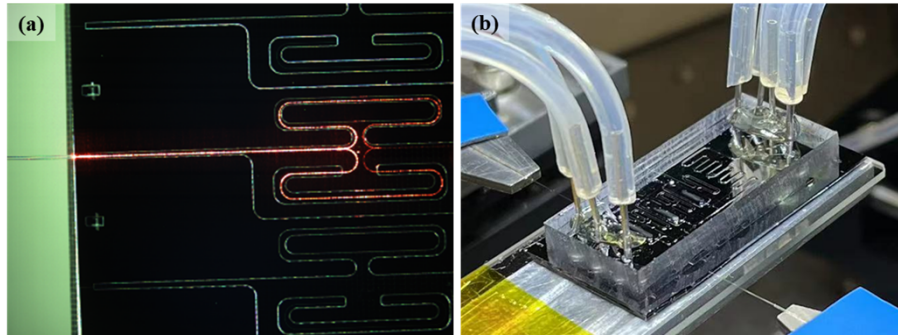


Fig. 3 Photo of a fabricated SU-8 optical waveguide MZI sensor (incident with red light) (a) Photo of an optofluidic chip vertically integrated with a PDMS microfluidic layer upon an optical waveguide chip.

If further consider the dependence of the effective refractive index of the working section of sensing arm on the refractive index of external medium, i.e., $\partial n_{e1}/\partial n_{ext}$, the bulk sensitivity S of the waveguide MZI sensor can be written as

$$S = \frac{FSR \cdot \tilde{L}_1}{\lambda} \cdot \frac{\partial n_{e1}}{\partial n_{ext}}, \quad (4)$$

where n_{ext} refers to the refractive index of external medium around the working section of sensing arm. In our design of MZI sensors, the length of the working section and embedded section of the sensing arm, i.e., \tilde{L}_1 and \tilde{L}_1 , and the length of reference arm L_2 are chosen to be 10.636 mm, 3.410 mm, and 13.918 mm, respectively. According to the numerical simulation, the group refractive indexes of the 2.1- μm wide sensing waveguide in water and the group

3.3. Transmission spectra of the fabricated MZI microsensors before and after packing with a microfluidic layer

The transmission spectra of the fabricated SU-8 optical waveguide MZI sensors before and after packing with microfluidic layer are shown in Fig. 4. The spectrum of MZI sensor before packaging is given in Fig. 4(a). It is not very flat in the wavelength range from 1530 nm to 1560 nm, which may result from the excitation of higher-order optical modes as the optical waveguide is designed to work at single-mode operation with Ormoclad cladding. For the waveguide of SiO₂/SU-8/air structure, the critical width for single mode operation is $\sim 2.4 \mu\text{m}$. After making a cladding of Ormoclad, the transmission spectrum of the MZI sensor becomes more regular and uniform as shown in Fig. 4(b). The FSR decreased from 7.3 nm to 4.2 nm. From Eqn. (2) and numerically calculated values of group refractive indexes, one can understand that such a decrease results from the change of n_{g2} from 1.6090 to 1.5805 (though its effective refractive index increased from 1.5213 to 1.5406), when its cladding layer is changed from air (whose refractive index is about 1.0) to Ormoclad (whose refractive index is about 1.52).

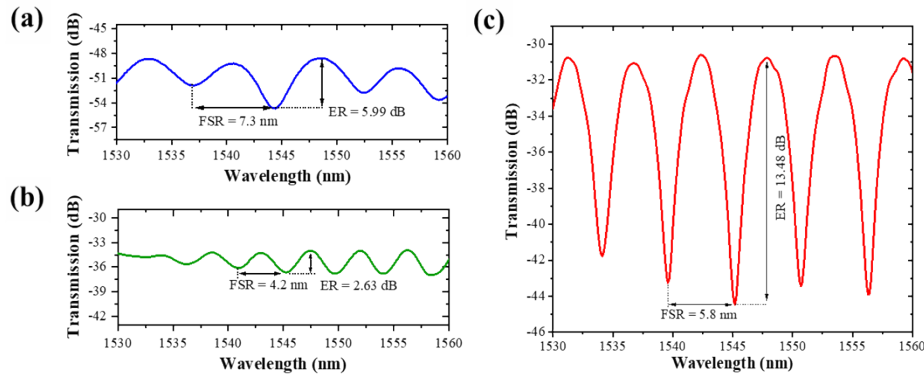


Fig. 4. Transmission spectra of the fabricated SU-8 waveguide MZI sensor. (a) Spectrum of the MZI sensor without cladding. (b) Spectrum of the MZI sensor after fabrication with Ormoclad cladding. (c) Spectrum of the MZI sensor in optofluidic chip after injection with water.

Figure 4(c) shows the measured transmission spectrum of the MZI sensor after packing with PDMS microfluidic layer and injecting water into the optofluidic chip. After injection of water into the sensing window, the FSR increased to 5.8 nm. From Eqn. (2) and numerically calculated values of group refractive indexes, one can understand that such a decrease results from the change of n_{g2} from 1.6090 to 1.5805 (though its effective refractive index increased from 1.5213 to 1.5406), when its cladding layer is changed from air (whose refractive index is about 1.0) to Ormoclad (whose refractive index is about 1.52). A more detailed comparison of the transmission spectra of MZI sensors using different Y splitters is given in Fig. S4. In Fig. S4(a), the 1:1 Y splitter is a symmetric design. The arc radius of 1:1 Y splitter is smaller than that of 1:2 Y splitter. It contributes to higher bending loss and thus a higher splitting ratio of 1:4 Y splitter. Compared with the results achieved by using the Y splitters with the splitting ratio of 1:1 and 1:4, the results achieved by using the Y splitter with the splitting ratio of 1:2 are the best. The extinction ratio of the MZI (ER) of both the 1:1 and 1:4 Y splitters is 2.63 dB and 13.48 dB, respectively. It is attributed to the specially designed Y splitter which can compensate the light propagation loss in the sensing arm and make the light powers from the two arms to be fairly close and thereby achieve a balanced interference at the output. A more detailed comparison of the transmission spectra of MZI sensors using different Y splitters is given in Fig. S4. In Fig. S4(a), the 1:1 Y splitter is a symmetric design. The arc radius of 1:1 Y splitter is smaller than that of 1:2 Y splitter. It contributes to higher bending loss and thus a higher splitting ratio of 1:4 Y splitter. Compared with the results achieved by using the Y splitters with the splitting ratio of 1:1 and 1:4, the results achieved by using the Y splitter with the splitting ratio of 1:2 achieved the highest extinction ratio.

Compared with the transmission spectra of the MZI sensor before and after fabrication of cladding, the optical power level of the transmission spectrum immersed in water has increased to some extent. It may be attributed to: 1) the eliminating of the excitation of high order modes after fabrication of Ormoclad cladding. As shown in the simulation result given in Fig. S5, the

order optical modes, such as TE_{21} and TM_{12} modes, occur only in the SU-8 waveguide with air cladding and disappear after changing the cladding from air to Ormoclad. 2) A better matching of optical waveguide modes at the interface around the edge of the sensing window after immersed in water. As the refractive index difference between Ormoclad and water is smaller than that between Ormoclad and air, the mode mismatching problem can thus be alleviated to depress optical loss. The simulation results in Fig. S6 revealed that the excess loss decreased from 0.329 dB to 0.066 dB when the cladding of the waveguide after the interface changes from air to water.

A long-time stability test of the fabricated polymer waveguide MZI sensor is shown in Fig. S7. Deionized (DI) water was injected into the sensing window of the packaged optofluidic chip in the test. The deviation of a peak wavelength of the transmission spectrum was measured for a long time over 2000 s. The standard deviation (SD) of the measured peak wavelengths is 30 pm.

3.4. Measurement of the bulk sensitivity of the fabricated MZI sensors

The bulk sensitivity of the fabricated MZI sensors was tested by using glucose solutions of different concentrations. A motorized syringe pump is used to inject and extract glucose solution into or out of the microfluidic channels. Figure 5(a) shows the measured wavelength shifts of the fabricated MZI sensor. It can be seen that the interference peak wavelength shifts to a longer wavelength with the increase of glucose concentration. Figure 5(b) presents the dependence of the wavelength shift of the MZI sensor on the external refractive indexes calculated by the concentrations of glucose solutions [33]. The inset shows the measured transmission spectra of the SU-8 waveguide MZI sensors in different glucose solutions. It reveals that the bulk sensitivity of the fabricated waveguide MZI sensor is 1695.95 nm/RIU, which is close to the estimated sensitivity, i.e., 1560 nm/RIU.

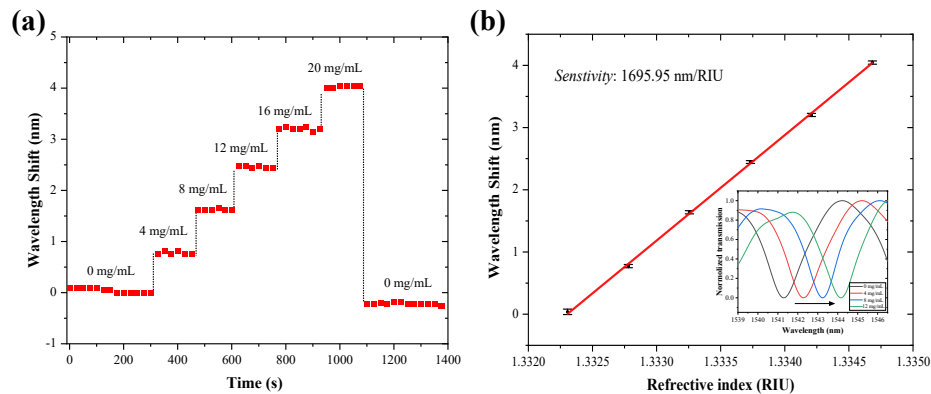


Fig. 5. Measured bulk sensitivity of the fabricated SU-8 waveguide MZI sensor: (a) Wavelength shift with respect to the concentration of glucose in water solution; (b) Wavelength shift with respect to the refractive index change. The inset shows the measured transmission spectra

decreased from 0.329 dB to 0.066 dB when the cladding of the waveguide after the interface changes from air to water.

A long-time stability test of the fabricated polymer waveguide MZI sensor is shown in Fig.

S7. Deionized (DI) water was injected into the sensing window of the packaged optofluidic

chip. The ability of the fabricated optofluidic chip in the detection of biochemical markers was

demonstrated by measuring the standard deviation of the measured peak wavelengths of the

30 pm and extracellular fluids and safeguards the human body against bacterial and viral infections

[30]. The waveguide MZI sensors were functionalized as depicted in Fig. 6(a). The surface of

SU-8 waveguide was activated to hydrophilic and then salinized with APTES and modified

with bulk sensitivity of the fabricated MZI sensors was tested by using glucose solutions of a

different concentrations. A motorized syringe pump was used to inject and extract glucose of

solution into or out of the microfluidic channels. Fig. 5a shows the measured wavelength shifts

of the fabricated MZI sensor. It can be seen that the interference peak wavelength shifts to a

longer wavelength with the increase of glucose concentration. Fig. 5b presents the dependence

of the wavelength shift of the MZI sensor on the external refractive indexes calculated by the

concentrations of glucose solutions [33]. The inset shows the measured transmission spectra of

the SU-8 waveguide MZI sensors in different glucose solutions. It reveals that the bulk

sensitivity of the fabricated waveguide MZI sensor is 1695.95 nm/RIU, which is close to the

estimated sensitivity, i.e., 1560 nm/RIU.

the experiment data. It can be seen that the 90%-response time of the sensor is about 257 s, and the total wavelength shift is about 0.33 nm. The measured wavelength shifts of the MZI biosensors in the HlgG solutions of different concentrations, including 0 ng/mL, 1 ng/mL, 10 ng/mL, 100 ng/mL, 200 ng/mL, 500 ng/mL, and 1000 ng/mL, are shown in Fig. 6(c). The inset presents their corresponding transmission spectra. By using the triple of standard deviation, the noise-estimated limit of detection (LOD) is 267 pg/mL, corresponding to 1.78 pM. This value is comparable or exceeds most of same type sensors reported by other researchers [19,23,30].

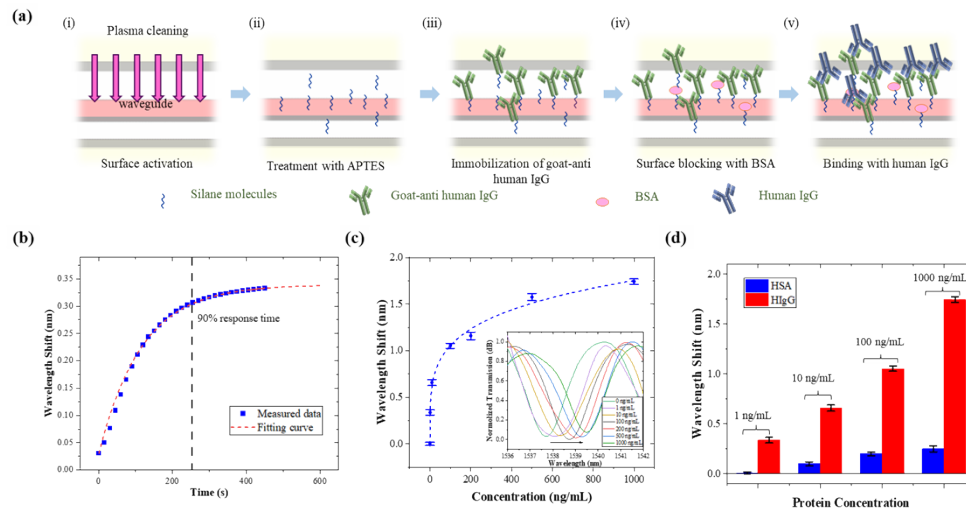


Fig. 6. (a) Schematic of the surface functionalization for detection of HlgG. (b) Dynamic response of the biosensor to target antigen. (c) Response of the biosensor to different concentrations of target antigen. (d) Comparison of the sensor's responses to control protein HSA and target analyte HlgG.

The specificity of the MZI biosensor was tested by comparison of the biosensor's responses to the target analyte HlgG and the human serum albumin (HSA), serving as a negative control. As shown in Fig. 6(d), the measured responses of the biosensor to HSA at a concentration of 1 ng/mL, 10 ng/mL, 100 ng/mL, and 1000 ng/mL are 0.029, 0.152, 0.19, and 0.143 times of these corresponding responses to HlgG at the same concentrations; which indicate a good selectivity of the MZI biosensor.

4. Discussion and conclusion

4. Discussion and conclusion

The polymer optical waveguide MZI sensor-based optofluidic biochip is a general label-free biosensing platform that can be applied to detect various kinds of biomarkers. As HlgG is a widely-plasma disease biomarker, we demonstrate the detection of HlgG to show the biocompatibility of the fabricated optofluidic chip. Further considering that IgG molecules are relatively large (whose molecular weight is 150 kDa) and the binding of smaller protein biomarkers on a surface usually leads to a larger change of refractive index [34], one may anticipate that our MZI sensor-integrated optofluidic chip can detect a wide variety of protein biomarkers. It is also believed that similar processes can be extended for other biological analysis, such as the testing of nucleic acid or virus etc. [35].

Notably, the optofluidic chip can be repeatedly used in multiple measurements. Using an antibody stripping solution, the HlgG layer can be eluted from the sensor surface after one detection. Figure 7 shows a testing result for the repeated use of a MZI biosensor for 5 cycles. After a detection process, the MZI sensor was incubated in an antibody-stripping solution for 30

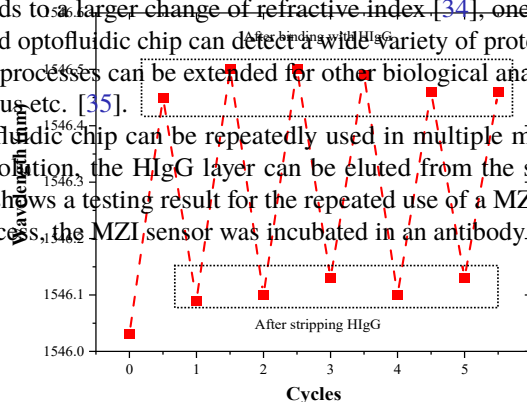


Fig. 7. Measured interference peak wavelengths of a fabricated optical MZI biosensor in 5 cycles of detection of HlgG.

1. Discussion and conclusion

The polymer optical waveguide MZI sensor-based optofluidic biochip is a general label-free biosensing platform that can be applied to detect many kinds of diseases biomarkers. As HlgG is a widely used disease biomarker, we demonstrated the detection of HlgG to show the biotransformation ability of the fabricated optofluidic chip. Further considering that IgG molecules are relatively large (whose molecular weight is 150 kDa) and the binding of smaller protein sensitivity didn't show any significant change in 5 cycles of testing.

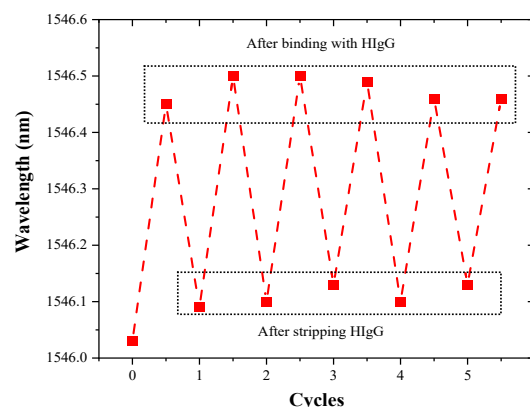


Fig. 7. Measured interference peak wavelengths of a fabricated optical MZI biosensor in 5 cycles of detection of HlgG.

In conclusion, we have presented an integrated optofluidic biochip with directly printed polymer optical waveguide MZI sensors. Asymmetric MZI sensors based on width-tailored waveguide have been designed and directly printed by using a digital UV lithography for high-sensitivity biosensing. After vertical integration with a microfluidic layer, an optofluidic chip has been demonstrated for on-chip biotransformation. Experimental results showed that the bulk sensitivity of the on-chip integrated MZI sensors is as high as 1695.95 nm/RIU and it can detect HlgG at the concentration level of 1.78 pM. Such a small-size high-performance optofluidic chip with reusable MZI biosensors has great potential in the development of miniature point-of-care diagnostic instruments and devices.

Funding. Research Grants Council of the Hong Kong Special Administrative Region, China (Grant No. 15220721).

Disclosures. There are no conflicts to declare.

Data availability. Data underlying the results presented in this paper are not publicly available at this time but may be obtained from the authors upon reasonable request.

Supplemental document. See [Supplement 1](#) for supporting content.

References

1. P. K. Drain, E. P. Hyle, F. Noubary, *et al.*, "Diagnostic point-of-care tests in resource-limited settings," *Lancet Infect. Dis.* **14**(3), 239–249 (2014).
2. B. Gil Rosa, O. E. Akingbade, X. Guo, *et al.*, "Multiplexed immunosensors for point-of-care diagnostic applications," *Biosens. Bioelectron.* **203**, 114050 (2022).
3. T. Chalyan, R. Guider, L. Pasquardini, *et al.*, "Asymmetric Mach-Zehnder interferometer based biosensors for aflatoxin M1 detection," *Biosensors* **6**(1), 1 (2016).
4. E. Stern, A. Vacic, N. K. Rajan, *et al.*, "Label-free biomarker detection from whole blood," *Nat. Nanotechnol.* **5**(2), 138–142 (2010).
5. Z. Wang, J. Zhao, X. Xu, *et al.*, "An overview for the nanoparticles-based quantitative lateral flow assay," *Small Methods* **6**(1), 2101143 (2022).
6. G. A. Posthuma-Trumpie, J. Korf, and A. van Amerongen, "Lateral flow (immuno)assay: its strengths, weaknesses, opportunities and threats: a literature survey," *Anal. Bioanal. Chem.* **393**(2), 569–582 (2009).
7. C. Parolo, A. Sena-Torralba, J. F. Bergua, *et al.*, "Tutorial: design and fabrication of nanoparticle-based lateral-flow immunoassays," *Nat Protoc* **15**(12), 3788–3816 (2020).
8. C. Huang, T. Wen, F.-J. Shi, *et al.*, "Rapid detection of IgM antibodies against the SARS-CoV-2 virus via colloidal gold nanoparticle-based lateral-flow assay," *ACS omega* **5**(21), 12550–12556 (2020).

9. D. Barshilia, L.-K. Chau, and G.-E. Chang, "Low-cost planar waveguide-based optofluidic sensor for real-time refractive index sensing," *Opt. Express* **28**(19), 27337 (2020).
10. J. W. Parks, H. Cai, L. Zempoaltecatl, *et al.*, "Hybrid optofluidic integration," *Lab Chip* **13**(20), 4118 (2013).
11. G. G. Meena, A. Jain, J. W. Parks, *et al.*, "Integration of sample preparation and analysis into an optofluidic chip for multi-target disease detection," *Lab Chip* **18**(23), 3678–3686 (2018).
12. D. Yin, E. J. Lunt, M. I. Rudenko, *et al.*, "Planar optofluidic chip for single particle detection, manipulation, and analysis," *Lab Chip* **7**(9), 1171 (2007).
13. Q. Liu, J. Nam, S. Kim, *et al.*, "Two-stage sample-to-answer system based on nucleic acid amplification approach for detection of malaria parasites," *Biosens. Bioelectron.* **82**, 1–8 (2016).
14. X. Ouyang, T. Liu, Y. Zhang, *et al.*, "Ultrasensitive optofluidic enzyme-linked immunosorbent assay by on-chip integrated polymer whispering-gallery-mode microlaser sensors," *Lab Chip* **20**(14), 2438–2446 (2020).
15. S. Yun, S. Park, B. Park, *et al.*, "Polymer-waveguide-based flexible tactile sensor array for dynamic response," *Adv. Mater.* **26**(26), 4474–4480 (2014).
16. P. Kozma, F. Kehl, E. Ehrentreich-Förster, *et al.*, "Integrated planar optical waveguide interferometer biosensors: a comparative review," *Biosens. Bioelectron.* **58**, 287–307 (2014).
17. A. Gaston, I. Lozano, F. Perez, *et al.*, "Evanescent wave optical-fiber sensing (temperature, relative humidity, and pH sensors)," *IEEE Sensors J.* **3**(6), 806–811 (2003).
18. N. Zhong, Q. Liao, X. Zhu, *et al.*, "Temperature-independent polymer optical fiber evanescent wave sensor," *Sci Rep* **5**(1), 11508 (2015).
19. P. Ramirez-Priego, D. Martens, A. A. Elamin, *et al.*, "Label-free and real-time detection of tuberculosis in human urine samples using a nanophotonic point-of-care platform," *ACS Sens.* **3**(10), 2079–2086 (2018).
20. A. Densmore, M. Vachon, D.-X. Xu, *et al.*, "Silicon photonic wire biosensor array for multiplexed real-time and label-free molecular detection," *Opt. Lett.* **34**(23), 3598 (2009).
21. M. Angelopoulou, P. S. Petrou, E. Makarona, *et al.*, "Ultrafast multiplexed-allergen detection through advanced fluidic design and monolithic interferometric silicon chips," *Anal. Chem.* **90**(15), 9559–9567 (2018).
22. R. Bruck, E. Melnik, P. Muellner, *et al.*, "Integrated polymer-based Mach-Zehnder interferometer label-free streptavidin biosensor compatible with injection molding," *Biosens. Bioelectron.* **26**(9), 3832–3837 (2011).
23. P. Azuelos, P. Girault, N. Lorrain, *et al.*, "High sensitivity optical biosensor based on polymer materials and using the Vernier effect," *Opt. Express* **25**(24), 30799 (2017).
24. A. del Campo and C. Greiner, "SU-8: a photoresist for high-aspect-ratio and 3D submicron lithography," *J. Micromech. Microeng.* **17**(6), R81–R95 (2007).
25. A. Landowski, D. Zepp, S. Wingerter, *et al.*, "Direct laser written polymer waveguides with out of plane couplers for optical chips," *APL Photonics* **2**(10), 106102 (2017).
26. Y. Xin, G. Pandraud, Y. Zhang, *et al.*, "Single-mode tapered vertical SU-8 waveguide fabricated by e-beam lithography for analyte sensing," *Sensors* **19**(15), 3383 (2019).
27. Z. Ding, H. Wang, T. Li, *et al.*, "Fabrication of polymer optical waveguides by digital ultraviolet lithography," *J. Lightwave Technol.* **40**(1), 163–169 (2022).
28. J. Wu, X. Guo, A. P. Zhang, *et al.*, "Rapid 3D μ -printing of polymer optical whispering-gallery mode resonators," *Opt. Express* **23**(23), 29708 (2015).
29. D. Dai, B. Yang, L. Yang, *et al.*, "Compact microracetrack resonator devices based on small SU-8 polymer strip waveguides," *IEEE Photonics Technol. Lett.* **21**(4), 254–256 (2009).
30. E. Melnik, R. Bruck, P. Müellner, *et al.*, "Human IgG detection in serum on polymer based Mach-Zehnder interferometric biosensors," *J. Biophoton* **9**(3), 218–223 (2016).
31. M. Kitsara, K. Misiakos, I. Raptis, *et al.*, "Integrated optical frequency-resolved Mach-Zehnder interferometers for label-free affinity sensing," *Opt. Express* **18**(8), 8193 (2010).
32. X. Jiang, Y. Chen, F. Yu, *et al.*, "High-sensitivity optical biosensor based on cascaded Mach-Zehnder interferometer and ring resonator using Vernier effect," *Opt. Lett.* **39**(22), 6363 (2014).
33. Y.-L. Yeh, "Real-time measurement of glucose concentration and average refractive index using a laser interferometer," *Optics and Lasers in Engineering* **46**(9), 666–670 (2008).
34. J. Vörös, "The density and refractive index of adsorbing protein layers," *Biophys. J.* **87**(1), 553–561 (2004).
35. P. Damborský, J. Švitel, and J. Katrlík, "Optical biosensors," *Essays in Biochemistry* **60**(1), 91–100 (2016).